AIChE

Batch-to-Batch Control of Characteristic Points on the PSD in Experimental Emulsion Polymerization

Mustafa T. Dokucu and Francis J. Doyle III
Dept. of Chemical Engineering, University of California, Santa Barbara, CA 93106

DOI 10.1002/aic.11618
Published online October 24, 2008 in Wiley InterScience (www.interscience.wiley.com).

An integrated batch-to-batch and in-batch control algorithm to regulate the endpoint particle size distribution (PSD) in an experimental semibatch emulsion copolymerization reactor is presented. Partial least squares (PLS) models of the process are utilized in a model predictive control (MPC) framework to regulate the PSD. The high dimensionality of the PSD is reduced through the use of a new approach, where the heights and positions of the characteristic points on the distribution are used to represent the whole distribution. This approach enables one to shift control priorities on the positions of the modes of a distribution with respect to the heights of the modes as well as efficiently reducing the dimensionality of the problem. The proposed algorithm is first tested on the simulation of the plant and showed success in regulating the PSD both in set point changes and against persistent disturbances. The experimental validation of the algorithm included two case studies where the controller was found to be effective.
 AIChE J, 54: 3171–3187, 2008
Keywords: population balance model, particle size distribution, emulsion polymerization, model predictive control, partial least squares regression

Introduction

The regulation of the distributions in particulate systems is critical due to the strong correlation between end product quality and the distributed properties. In many industrial applications, the desired distribution has a complex shape that increases the need for efficient regulation of the end product distributions. The complex shape of the distribution prohibits the use of average properties (e.g., mean of the distribution, moments) as controlled outputs and the regulation of the full distribution is motivated. Emulsion polymerization, the particulate process that is considered in this work, is an essential particulate process for carrying out free radical polymerization in a safe and environmentally benign approach while achieving high molecular weights and high conversions. The control of the particle size distribution (PSD) in emulsion polymerization is essential due to the close relationship between the morphological properties of the emulsion product and the PSD.[1–4]

The modeling of the evolution of the PSD requires an understanding of the growth, nucleation, and the coagulation phenomena and their interactions. Therefore, it is necessary to use population balance equations (PBE) when modeling the evolution of the PSD in particulate processes. Population balance models and the numerical solution of the PBEs have been an active area of research and the interested reader is referred to the review by Kiparissides[5] and the book by Ramkrishna.[6] The control of emulsion polymerization reactors has been reviewed by Dimitratos et al.[7] and more recently, Richards and Congalidis[8] reviewed the measurement and control of polymerization reactors. One of the main themes in both of these reviews is the need for frequent on-line measurements for the control of the emulsion polymerization reactors. The difficulty of feedback control of the

Correspondence concerning this article should be addressed to F. J. Doyle at doyle@engineering.ucsb.edu.

PSD in emulsion polymerization systems has stimulated reachability studies on emulsion polymerization and PBE systems. Semino and Ray[9,10] assessed the controllability of the PBE systems with undistributed actuators. They found that the use of feed concentrations of surfactant and initiators guaranteed the controllability of emulsion polymerization systems in the unconstrained problem. Wang and Doyle[11] studied the reachability of unimodal and bimodal PSDs in semibatch styrene emulsion polymerization and showed the change of the reachable PSD space with changing batch duration and initial reaction conditions. They also highlighted the importance of early corrective action in the case of midcourse correction (MCC) control policies. Although, the population balance models provide a deep understanding of particulate processes, their direct inclusion in a model-based framework brings computational and parameter identification challenges. Therefore, another recurring theme in the PSD control literature has become the model reduction of the infinite dimensional distribution(s). In some approaches, the dynamic behavior of the infinite-dimensional system is regulated through the model-based control of the reduced-order characteristic, moments of the PSD.[12–14] The moment model-based control approach is feasible when the desired properties of the size distribution can be accurately described by the moment model of the PBE system. Crowley et al.[15] controlled the full PSD in a semibatch styrene emulsion polymerization reactor. Surfactant feed rate profile and free surfactant profile were considered and compared as manipulated variables. They concluded that the use of the free surfactant profile provided better control over nucleation events and thus resulted in better PSD control. Lee et al.[16] studied the control of PSD in a simulated semibatch calcium carbonate precipitation reactor, where they compared the performances of batch-to-batch, on-line, and integrated batch-to-batch and on-line controllers to shape the endpoint PSD of the precipitated calcium carbonate. The model-based on-line controller that utilized the closed-form solution to the PBE system integrated with a batch-to-batch controller was found to give the best performance. Doyle et al.[17] described the deviation of a nonlinear process model from the simulated virtual process plant by using a partial least squares (PLS) model and controlled the endpoint PSD of an emulsion polymerization system with a sequential quadratic programming (SQP) based algorithm. Flores-Cerrillo and MacGregor[18] combined within-batch and batch-to-batch control strategies to control the full PSD (discrete values at 60 size classes) in a simulated styrene emulsion polymerization model developed by Crowley et al.[15] Their methodology uses the batch-to-batch and current batch information to adjust the magnitudes of surfactant shots to reject disturbances during the batch and to track the set point changes. The control computations are established through a model-based minimum-variance controller with a detuning factor utilizing partial-least square models of the simulated system. Park et al.[19] used a PLS model-based predictive controller that utilized on-line measurements of the PSD during a batch to predict and regulate the endpoint PSD in an experimental semibatch emulsion copolymerization reactor. Alhamad et al.[20] used a dynamic matrix controller to regulate the average radius, particle size polydispersity index, average molecular weight, and monomer conversion in an experimental styrene/MMA emulsion copolymerization reactor. Rajabi-Hamane and Engell[21] explored the time optimal operation of a seeded emulsion polymerization reactor to achieve a target PSD. The monomer feed rate was manipulated to minimize the batch time while achieving a target PSD with heat removal and maximum monomer constraints in the simulation study. The controller used variable controller intervals that were found to be beneficial for the performance.

In summary, there are three categorical approaches utilized for the control of a semibatch system: batch-to-batch control, in-batch on-line feedback control and integrated algorithms that combine these two methods. It is crucial to utilize the historic batch information to correct for persistent, systematic disturbances in batch processes. This can be achieved by a batch-to-batch methodology that uses data from prior batches to formulate the operation of the next batch. The goal of this reformulation is to move the quality variable (e.g., PSD) to a target zone that would be desirable for economical purposes. The algorithm that is presented in this work aims to optimize the batch formulation from each batch to the next batch (batch-to-batch) while also employing an in-batch on-line component regulating the system against unmeasured, random disturbances. The controller does not utilize the PBE model of the process, but instead it utilizes empirical models constructed by using past on-line process data. Another aspect that is distinct from the previous approaches is the treatment of the high-dimensional PSD data. Rather than representing the PSD with principal components, moments, or integral quantities concentrated at pivot sizes, the PSD is represented and reduced by the characteristic points selected on the distribution. These characteristic points are called the "tracer elements" in this work. The tracer elements are characterized by using a specific property, such as the maximum or minimum point at a size range, exhibited by the distribution. The definition of the tracer elements is flexible and may be designed to reflect the specific properties required from a distribution. Once a tracer element is located, it is characterized by two variables: its location on the size axis (x-axis) and its weight fraction (y-axis). This novel representation lets effective formulation of the objective function to be minimized apart from reducing the PSD to a smaller number of variables. The relationship between the input changes and the tracer elements is captured by a PLS model in this study. It must be noted that the main aim in this study is to regulate the PSD. The regulation of important variables such as the co-polymer composition and the total polymer mass is not addressed, although the methodology is general enough to accommodate these constraints. Since the regulation of co-polymer composition and polymer mass through appropriate input constraints would restrict the reachable PSD zone, these constraints were not included in the formulation in order to better assess the developed methodology's effectiveness in shaping the endpoint PSD.

The article is organized as follows. The next section "Representation and Reduction of the Particle Size Distribution" will introduce the tracer element concept. The controller algorithm and the utilization of PLS are presented in the "Controller Methodology" section. The next section, "Semibatch VAc/BuA Emulsion Copolymerization System," describes the experimental and the simulated systems. The performance of the batch-to-batch algorithm is illustrated

with simulated disturbance scenarios in the following section "Simulation Case Studies". The experimental validation of the proposed algorithm is presented in two case studies in the "Experimental Case Studies" section. Finally, the performance of the proposed approach is summarized in the "Conclusions".

Representation and Reduction of the Particle Size Distribution

The representation of the PSD is accomplished through the use of characteristic points that are denoted "tracer elements" to represent the distribution for particular size ranges. The weight averaged PSD, $w_{\mathrm{PSD}}(d)$, is assumed to be a smooth function of the particle size, d. This assumption is quite realistic as many size distribution devices (e.g., the one used in this work) detect particle populations at discrete sizes and fit smooth distribution functions to these clusters of particles to represent the whole particle population. The identification of the tracer elements that depict the main characteristics of a distribution is flexible and depends upon the specific distribution that is considered. Here, the identification of the tracer elements in the case of a bimodal distribution is used as an example. Two size ranges are used to define the two modes of the PSD by the tracer elements. The diameter size that corresponds to the maximum point of the distribution in each size range is determined as shown in Eq. 1.

$$y_{\mathrm{pos},2} = \arg\max_{d}\left(\max_{d_{\mathrm{min},1}\le d<d_{\mathrm{max},1}} w_{\mathrm{PSD}}(d)\right) \tag{1}$$

The bi-level maximization in the Eq. 1 is necessary for distinguishing between two or more points on the distribution that have the same maximum value for that size range (e.g., in the case of a saddle point). Although maximum operators are utilized in this work, operators such as the minimum operator can also be used. The main idea behind the selection of the tracer elements is to capture important and economically relevant characteristics of the target or the evolving distribution. Once the first tracer element has been defined for a size range, two other points are selected, which are at a predefined distance from the diameter size, $y_{\mathrm{pos},2}$, as shown below in Eq. 2.

$$\begin{aligned} y_{\mathrm{pos},1} &= y_{\mathrm{pos},2} - s_1 \\ Y_{\mathrm{pos},3} &= y_{\mathrm{pos},2} + s_2 \\ y_{\mathrm{hei},1} &= w_{\mathrm{PSD}}(y_{\mathrm{pos},1}) \\ y_{\mathrm{hei},2} &= w_{\mathrm{PSD}}(y_{\mathrm{pos},2}) \\ y_{\mathrm{hei},3} &= w_{\mathrm{PSD}}(y_{\mathrm{pos},3}) \end{aligned} \tag{2}$$

In Eq. 2, the parameters s_1 and s_2 characterize the spread of the distribution around the tracer element of size, $y_{\mathrm{pos},2}$, and weight fraction, $y_{\mathrm{hei},2}$. The location of the characteristic points for the case of two size ranges and three tracer elements for each size region is depicted in Figure 1.

A certain degree of expertise is essential to determine the computation of these tracer elements. Although a systematic procedure for the selection of tracer elements would be ideal, this procedure would be closely related to the mapping between the specific particulate product and the size-distribution, which is an open problem in the literature. However, since a statistical model of the process will be utilized in this work, training data will already be available. The calibration data provide insight to determine the important parameters for the definition of the tracer elements, such as the number of tracer points for each size region, the upper and lower limits of the size ranges, and the size distance between the elements. The characterization of each tracer element by its size and its fraction allows for an efficient formulation of an objective function in a model predictive control (MPC) framework. For example, a large penalty might be introduced to the deviations from the target tracer element positions compared with the deviations from the target weight fractions (heights). The tracer element approach is also an efficient technique to reduce the dimensionality of the PSD to a sufficient number of variables describing the main characteristics.

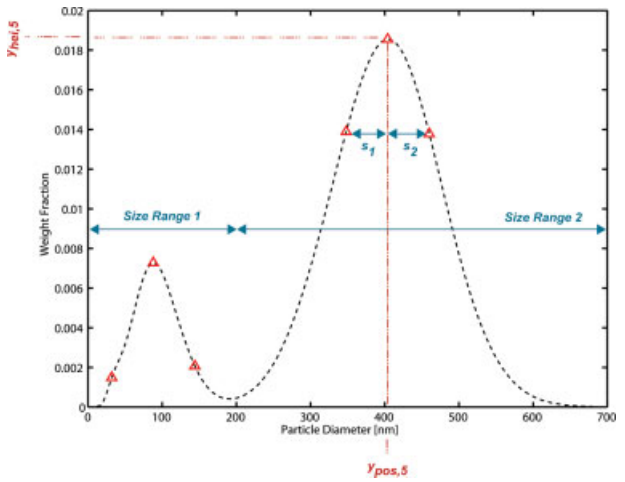

Figure 1. Graphical representation of the location of the tracer elements in the case of a bimodal distribution characterized by six tracer elements.

Two size regions are used where three tracer elements are defined for each size region. [Color figure can be viewed in the online issue, which is available at www.interscience.wiley.com.]

Controller Methodology

The main concept underlying the controller algorithm is the utilization of all the available information about the history of the batch process until the current point at each decision time. The information might be taken during the batch, or it may come from prior batches. There are one or more decision times in the proposed approach (if only one decision time is utilized, the controller is a traditional batch-to-batch controller). The zeroth decision time is before the batch and the rest of the decision times are during the batch. At these decision times, all the information (from previous batches and the current batch) up to and including the current decision time are used in a PLS model to predict the endpoint quality variables, i.e., tracer elements of the PSD. The decision times are fixed and not changed during the execution of the batch. The decision times can also be added as decision

variables to give more degrees of freedom to the controller and also allow for nonfixed batch time operations, which would require significant changes to the models used for predicting the end product properties. With a predictor of the final product properties of the current batch, it is possible to solve the associated dynamic optimization problem to minimize the deviation of the controlled outputs from their targets.

The endpoint outputs are predicted by specific PLS models at each decision time. PLS regression aims to capture the variances of predictor and quality variables and also achieves a correlation between these variables.[22] PLS also removes the high correlation that may exist in X_k, all the information available at a decision time k, by first projecting it to a lower dimensional principal component space. Principal component analysis (PCA) is also applied to the output space, Y, but in a way to maximize the covariance between X_k and Y. The input and output spaces and their decomposition in PLS framework are presented in Eq. 3.

$$\begin{aligned} X_k &= T_k P_k^T + E_k \\ Y &= U_k Q_k^T + F_k \end{aligned} \tag{3}$$

In Eq. 3, T_k and U_k are the score matrices, P_k and Q_k are the loading matrices, and E_k and F_k are the residual matrices of X_k and Y, respectively. The score matrix of X_k, T_k, is rotated by a diagonal matrix, B_k, to define the quality variables as shown in Eq. 4.

$$Y = T_k B_k Q_k^T + G_k \tag{4}$$

The diagonal elements of B_k are called the regression weights. These weights are selected to minimize the induced 2-norm of the residual matrix, G_k. There are two main methods for the calculation of these regression weights: nonlinear-iterative PLS (NIPALS)[22] and SIMPLS.[23] In this study, SIMPLS is preferred over NIPALS mainly because of its speed. SIMPLS is also slightly superior to the NIPALS algorithm since it explicitly maximizes the covariance between X_k and Y.[24] The PLS toolbox by Eigenvector Inc. was used for all the PCA applications in this section.[24] Details are omitted for the sake of brevity and the interested reader is referred to the original publications for further detail. If X_k is assumed to be $X_k = T_k P_k^T$, it follows from Eq. 4 that:

$$Y = X_k \beta_k + G_k \tag{5}$$

where β_k is $\beta_k = P_k (P_k^T P_k)^{-1} B_k Q_k^T$.

To obtain PLS models of the system, a training dataset including sufficient historic batch information is necessary. The predictor block with n_b batches and n_d decision times for the decision time $k > 0$ is:

$$X_k = \begin{bmatrix} y(1,1)^T & \cdots & y(1,k)^T & \Delta u(1,0)^T & \cdots & \Delta u(1,n_d)^T \\ \vdots & \ddots & \vdots & \vdots & \ddots & \vdots \\ y(n_b,-1)^T & \cdots & y(n_b,k)^T & \Delta u(n_b,0)^T & \cdots & \Delta u(n_b,n_d)^T \end{bmatrix} \tag{6}$$

where $y(i,k)$ is a vector that includes on-line measured output data of the batch i, and decision time k. Similarly, $u(i,k)$ is the vector of input changes for ith batch and kth decision time. The vector $y(i,k)$ includes the secondary variables and the tracer element positions and weight fractions from the past and current decision times.

$$y(i,k)^T = \begin{bmatrix} y_s(i,k) & y_{pos}(i,k)^T & y_{hei}(i,k)^T \end{bmatrix} \tag{7}$$

The predictor block for the zeroth decision time (before the current batch), X_0, consists only of the future input changes that are decided before the batch:

$$X_0 = \begin{bmatrix} \Delta u(1,0)^T & \cdots & \Delta u(1,n_d)^T \\ \vdots & \ddots & \vdots \\ \Delta u(n_b,0)^T & \cdots & \Delta u(n_b,n_d)^T \end{bmatrix} \tag{8}$$

The output block, Y, is the same for all the decision times, since only the endpoint tracer elements are included in it:

$$Y = \begin{bmatrix} y_{pos}(1,t_{end})^T & y_{hei}(1,t_{end})^T \\ \vdots & \vdots \\ y_{pos}(n_b,t_{end})^T & y_{hei}(n_b,t_{end})^T \end{bmatrix} \tag{9}$$

Since many of the variables have different units, all of the columns (corresponding to different variables) of the predictor and the output blocks are scaled to have zero mean and standard deviation of one. The associated PLS model, β_k can be constructed from each pair of input blocks, X_k, and the output block, Y. The multiway predictor block is unfolded horizontally as suggested in literature[25] in this work to build a different PLS model for each decision time, k, as shown in Figure 2.

The PLS model presented in Eq. 5 can be used at each decision time, k, to predict the final quality variables:

$$y^T = x_k^T \beta_k \tag{10}$$

where y consists of the predicted tracer elements of the endpoint distribution:

$$y^T = \begin{bmatrix} y_{pos}(i,k)^T & y_{hei}(i,k)^T \end{bmatrix} \tag{11}$$

The PLS model, β_k, is obtained from past batches and is applied to the current batch to predict the endpoint outputs using the predictor vector, x_k of the current batch. X_k includes past measurements and input changes as well as the future input changes. Once a batch is completed, X_k and Y can be augmented with the new data and the PLS models for each decision time can be reconstructed. One important parameter for PLS models is the number of latent variables. To select this important parameter, cross-validation methods are used to find the optimum number of latent variables giving the best prediction performance for each PLS model. Another important detail is the limit of expanding the PLS models with new batch data. Instead of using the complete history of batches to build the models, a moving window of most recent batches will be used in this work as suggested by Doyle et al.[17]

To develop the controller methodology, the regressor matrix is decomposed into two parts for the past and future values of the predictor variables:

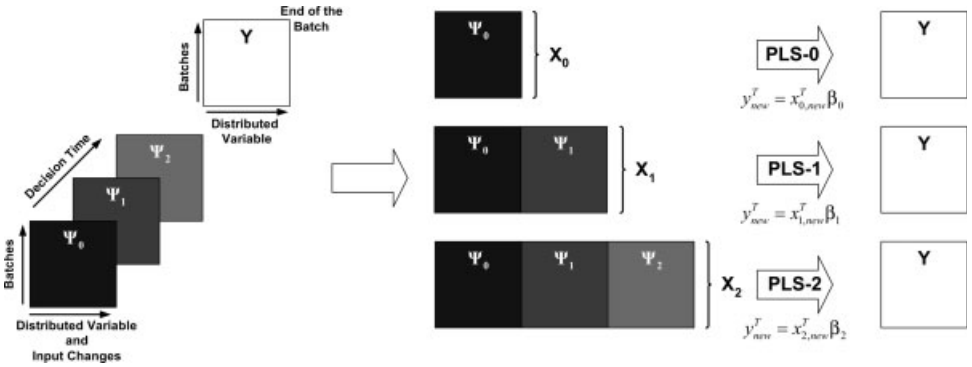

Figure 2. The unfolding of the multiway data that is applied in this work.

A different PLS model is constructed for each decision time before and during the batch.

$$y^T = \begin{bmatrix} x_{k,\text{past}}^T & x_{k,\text{future}}^T \end{bmatrix} \begin{bmatrix} \beta_{k,\text{past}} \\ \beta_{k,\text{future}} \end{bmatrix} \tag{12}$$

For the first decision time, which is before the beginning of the batch, there will be no past values of the predictor variables, so x_1 is set to $x_{k,\text{future}}$ and β_k is set to $\beta_{k,\text{future}}$. $x_{k,\text{past}}$ and $x_{k,\text{future}}$ are presented to clarify their definition for the third decision time of a sample batch, with four decision times in Eq. 13.

$$\begin{aligned} x_3^T &= \begin{bmatrix} y_1^T & y_2^T & y_3^T & \Delta u_0^T & \Delta u_1^T & \Delta u_2^T & \Delta u_3^T \end{bmatrix} \\ x_{3,\text{past}}^T &= \begin{bmatrix} y_1^T & y_2^T & y_3^T & \Delta u_0^T & \Delta u_1^T \end{bmatrix} \\ x_{3,\text{future}}^T &= \begin{bmatrix} \Delta u_2^T & \Delta u_3^T \end{bmatrix} \end{aligned} \tag{13}$$

It must be noted that the $x_{k,\text{future}}$ will always include the future input changes that will be introduced to the system. Thus, it will always be the decision variable vector of the designed objective function.

The development of an MPC controller with a quadratic objective function is straightforward. The goal of the controller is to minimize the deviation of the predicted output vector, y, from its target, y_{ref} while minimizing the control effort. The predicted endpoint error can be represented as:

$$y_{\text{ref}}^T - y^T = y_{\text{ref}}^T - x_{k,\text{past}}^T \beta_{k,\text{past}} - x_{k,\text{future}}^T \beta_{k,\text{future}} \tag{14}$$

In Eq. 14, $y_{\text{ref}}^T - x_{k,\text{past}}^T \beta_{k,\text{past}}$ is the future open-loop error of the system representing the endpoint error if no future input changes are made. With these definitions, the optimization problem with the quadratic objective function can be defined as:

$$\begin{aligned} \min_{x_{k,\text{future}}} \quad & \left\| \Gamma(y_{\text{ref}} - y) \right\|_2^2 + \left\| \Lambda x_{k,\text{future}} \right\|_2^2 \\ s.t. \quad & C^x x_{k,\text{future}} \geq c_k \end{aligned} \tag{15}$$

where C^x and c_k are used to define the lower, upper, and rate constraints on the inputs. This optimization problem can be converted to a standard quadratic programming (QP):

$$\begin{aligned} \min_{x_{k,\text{future}}} \quad & \frac{1}{2} x_{k,\text{future}}^T H x_{k,\text{future}} - G x_{k,\text{future}} \\ s.t. \quad & C^x x_{k,\text{future}} \geq c_k \end{aligned} \tag{16}$$

for which the Hessian and the gradient of the QP are:

$$\begin{aligned} H &= \beta_{k,\text{future}} \Gamma^T \Gamma \beta_{k,\text{future}}^T + \Lambda^T \Lambda \\ G &= \beta_{k,\text{future}} \Gamma^T \Gamma (y_{\text{ref}} - \beta_{k,\text{past}}^T x_{k,\text{past}}) \end{aligned}$$

The first element of $x_{k,\text{future}}$ (i.e., first element of future input changes) is implemented for the process and the optimization problem is reformulated and solved at the next decision time iteratively, utilizing the most current measurements. The inputs to the system at any time t are defined as:

$$u(t) = u^{\text{nom}(t)} + \sum_{i=1}^{\{k:\theta_{k+1} > t > \theta_k\}} \text{diag}(u^{\text{base}}) \Delta u_i \tag{17}$$

where u^{base} represents the base values of the manipulated inputs presented in Table 1, u^{nom} represents the trajectories of the manipulated variables for the nominal batch recipe and θ_k is the corresponding batch time of the kth decision time during the batch. In some of the published approaches,[18] a no-control zone is defined in terms of the reduced quality variable and no control action is taken unless these reduced variables fall out of the no-control zone. This might be desirable from an operational point of view. The zone can be defined in the low dimensional principal component space of the quality variables. In this work, no-control zones will not be utilized to highlight the performance and robustness of the proposed algorithm.

Table 1. Semibatch VAc/BuA Emulsion Copolymerization System Conditions

Initial Reactor Charge	
Water (L)	1.0
VAc (g)	26
Ferrous ammonium sulfate (g)	0.1
Sodium benzoate (g)	1.12
Reactor temperature (°C)	60

System Inputs	Base Value of the Input (u^{base}; $\times 10^{-3}$ mol/s)
VAc (u_1)	0.299
BuA	0.281
Surfactant (u_2)	0.710
tBHP	0.271
SFS	0.186

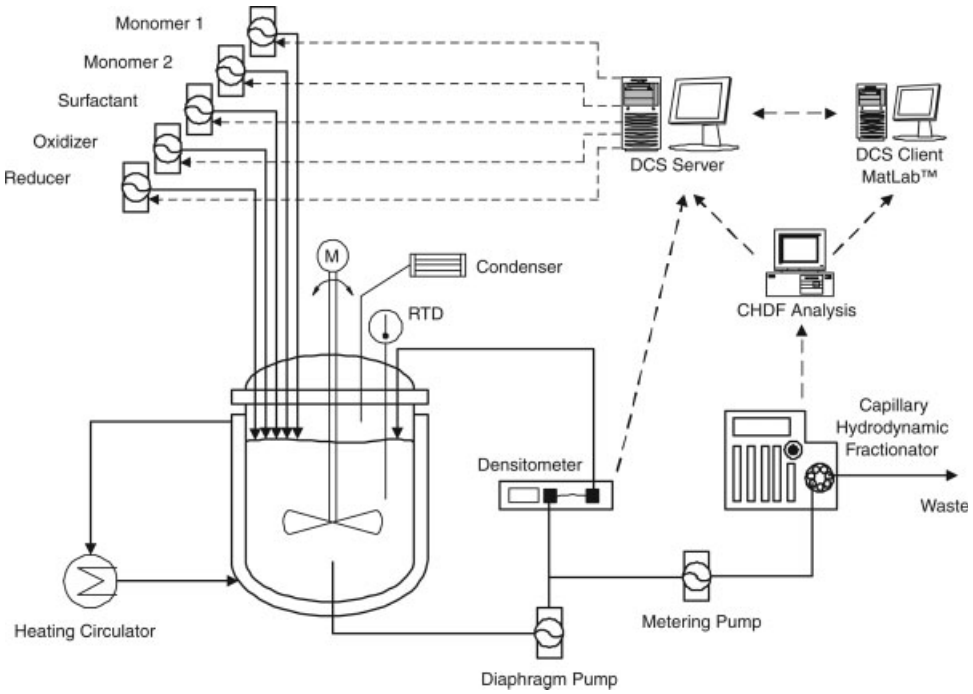

Figure 3. Closed-loop experimental setup.

The remote-setpoint precise metering pumps are operated by the DCS. The feed rates are determined by the controller that utilizes on-line PSD (CHDF) and density (densitometer) measurements.

Semibatch VAc/BuA Emulsion Copolymerization System

Closed-loop experimental system

The emulsion polymerization of vinyl acetate (VAc) and butyl-acrylate (BuA) is carried out with non-ionic surfactants in the system considered in this study. In normal operation, the system is run in an isothermal, semibatch fashion, although it is also possible to operate in a nonisothermal and/or batch mode. A schematic diagram of the experimental facility that is employed in this study is shown in Figure 3. The system consists of a 3 L borosilicate glass reactor, where the monomers, oxidizer, reducer, and the surfactant are delivered by remote set point metering pumps controlled by a Honeywell Plantscape™ distributed control system (DCS). The reactor is equipped with a jacket for adjusting the reactor temperature by the water coming from the heat bath. Mixing inside the reactor is obtained by the four vertical baffles and the agitator shaft. The head space is purged with nitrogen to maintain an inert environment throughout the reaction. A chiller, which is connected to a second heat bath, is attached to the top of the reactor to condense the exit purge gas and the vapors back to the reactor. To obtain on-line measurements, the latex is circulated through a sampling line at a fixed rate of 75 mL/min by a diaphragm pump. Density of the latex is measured by a densitometer installed on the sampling line. The densitometer infers the density of the latex from the frequency of vibration of the glass U-tube through which the latex passes. Following the exit from the on-line densitometer, a side stream from the sampling line is diluted by the eluant stream and directed to the capillary hydrodynamic fractionation (CHDF) for the PSD measurement. The eluant is a specific carrier fluid designed for fractionation purposes. Although almost all of the commercially available methods (microscopy, separative techniques, scattering techniques) are practically accurate for measuring unimodal latexes, capillary hydro dynamic fractionation (CHDF) is the most viable method for measuring complex distributions on-line.[26,27] CHDF was preferred for the control setup in this work over the scattering techniques, due to its higher resolution over a wider particle range. The PSD measurements can be obtained every 12 min from the CHDF with a 12-min measurement delay, and density measurements are available every 1 min from the densitometer with negligible delay. After the side stream is taken from the sample line, the remaining sample in the loop is returned to the reactor, so that the material balance is not affected by the sampling loop. Flow rates of the reactants are measured by the flow sensors that are attached to the pumps or may be inferred from the load cells that measure the weights of the feed burettes. The DCS transmits all reactor data to the main computer, which communicates with the control computer using Microsoft Excel Data Exchange (MEDE). The control computer obtains the PSD measurements from the analysis computer through TCP/IP and calculates actual weight-averaged PSD from the relative size distribution provided by the CHDF. The analysis computer is connected to and administers the CHDF. The control algorithm presented in "Controller Methodology" section is coded in Matlab™ to determine the future values of manipulated inputs. These values of the manipulated variables are then conveyed to MEDE using the standard control communication protocol, Dynamic Data Exchange (DDE), and actuated by the DCS through low-level proportional integral control loops for the pumps. The system has precise remote-set point pumps that are basically reciprocating pumps but operating without valves.

In this study, the monomers butyl acrylate (BuA) and vinyl acetate (VAc) are used to produce polymer particles. The surfactant is a non-ionic one and the initiation of the polymerization is achieved by a redox pair. The redox pair consists of the oxidizer *t*-butyl hydrogen peroxide (tBHP) and the reducer sodium formaldehyde sulfoxylate (SFS), with ferrous ammonium sulfate added as the coordinating agent. The redox initiation mechanism allows low temperature initiation and provides more flexibility in the recipe formulation. In batch polymerizations, the BuA is polymerized much faster than the VAc. The more hydrophobic, softer BuA is in the core of the polymer particles while the more hydrophilic VAc constitutes the hard shell.

To produce particles where BuA is more homogeneously concentrated in the particles, BuA and VAc are fed slowly to the reactor. The low flow rates of the monomers coupled with the agitation prohibits the formation of a monomer droplet phase and minimizes the unreacted monomer inside the reactor. If the considered batch recipe has a potential for forming a separate monomer phase then and the unreacted monomer should be monitored and controlled.[28,29] The initial conditions of the system and the base flow rates of the monomers, surfactant, and the redox initiator pair are summarized in Table 1.

Analysis of the solids content

The density measurements that are available every minute are used to estimate the solids content. The total volume of the reactants in the reactor is calculated using the density of the latex:

$$V_T = V_{\mathrm{m1}} + V_{\mathrm{m2}} + V_{\mathrm{p}} + V_{\mathrm{w}} + V_{\mathrm{surf}} = m_T/\rho_{\mathrm{latex}} \tag{18}$$

The volume change of mixing at the beginning of the batch (V_{mix}) can be assumed to be constant throughout the batch that is computed as in Eq. 19.

$$\Delta V_{\mathrm{mix}} = V_T - V_{\mathrm{m1}} - V_{\mathrm{m2}} - V_{\mathrm{w}} - V_{\mathrm{surf}} \tag{19}$$

The initial change of mixing can be used to correct Eq. 18. In Eq. 18, the volume of water (V_{w}) and surfactant (V_{surf}) inside the reactor are known from the load cell measurements. The volume of the unreacted monomers (V_{mi}) and the volume of the polymer (V_{p}) inside the reactor are unknown and must be determined. Since the total mass of monomers added to the system ($m_{\mathrm{mi}}^{\mathrm{T}}$) is constantly measured, the mass of the polymer inside can be related to the unreacted monomer volumes,

$$m_{\mathrm{m1}}^{\mathrm{T}} + m_{\mathrm{m2}}^{\mathrm{T}} = V_{\mathrm{p}}\rho_{\mathrm{p}} + V_{\mathrm{m1}}\rho_{\mathrm{m1}} + V_{\mathrm{m2}}\rho_{\mathrm{m2}} \tag{20}$$

The ratio of the conversions of the monomers can be used to derive another relation between V_{m1} and V_{m2},

$$\frac{\left(V_{\mathrm{m1}}^T - V_{\mathrm{m1}}^T\right)\rho_{\mathrm{m1}}}{\mathrm{MW}_1} = r_{\mathrm{m}}\frac{\left(V_{\mathrm{m2}}^T - V_{\mathrm{m1}}^T\right)\rho_{\mathrm{m2}}}{\mathrm{MW}_2} \tag{21}$$

where the ratio of the reaction rates of the monomers, r_{m}, is defined as:

$$r_{\mathrm{m}} = \frac{k_{p_{11}}p_1[\mathrm{M}_1]_{\mathrm{p}} + k_{p_{21}}p_2[\mathrm{M}_1]_{\mathrm{p}}}{k_{p_{12}}p_1[\mathrm{M}_2]_{\mathrm{p}} + k_{p_{22}}p_2[\mathrm{M}_2]_{\mathrm{p}}} \tag{22}$$

The concentration of the monomers in the particle phase, $[\mathrm{M}_i]_{\mathrm{p}}$, is calculated by a partitioning equation, which is as follows:

$$[\mathrm{M}_i]_{\mathrm{p}}V_{\mathrm{p}}^s + \frac{[\mathrm{M}_i]_{\mathrm{p}}}{K_{p_i}}V_w + \frac{[\mathrm{M}_i]_{\mathrm{p}}}{K_{d_i}}V_{\mathrm{d}} = \frac{V_{\mathrm{m}i}\rho_{\mathrm{m}i}}{\mathrm{MW}_i} \qquad i = 1, 2 \tag{23}$$

where the swollen volume of the particles (V_{p}^s) is defined as:

$$V_{\mathrm{p}}^s = \frac{V_{\mathrm{p}}}{1 - \sum_{i=1}^{2}[\mathrm{M}_i]_{\mathrm{p}}\mathrm{MW}_i/\rho_{\mathrm{m}i}} \tag{24}$$

The volume of the monomer droplets, V_{d}, in Eq. 23 can be found by using the monomer concentration in the particle phase and the partition coefficients. However, in this study it is assumed that there is no separate monomer phase since the monomer flow rates are very low. Solids content, which is the ratio of the mass of the particles to the mass of the total reactants, can be calculated by solving the system of equations of Eqs. 18, 20, 21, and 23 for the unknown variables (V_{mi}, V_{p}, and $[\mathrm{M}_i]_{\mathrm{p}}$, for $i = 1$ and 2).

Simulated System

A population balance equation (PBE) model developed by Immanuel et al.,[30] that describes the evolution of the PSD in the emulsion polymerization system is used as a plant for the simulation case studies. The developed controller was first tested on this simulated plant prior to the experimental case studies. The model considers size dependent growth, partitioning of the nonionic surfactants, and the average number of radicals per particle calculations via first principles. A computationally efficient numerical method[31] that exploits the different inherent time scales present in emulsion polymerization is used to solve the particle PBE, where the PSD is discretized into 250 finite elements of 2 nm width spanning from 2 to 500 nm. This method relies on accounting for the nucleation, growth, and coagulation events individually in each element to update an integral amount particle distribution at each time.

In the simulation studies, the endpoint PSD of a nominal batch is used as the target for the closed-loop controllers that try to regulate to this target against disturbances. The input profiles for this nominal batch are presented in Figure 4. The evolution of the PSD with time is presented in Figure 5 when the nominal input profiles of Figure 4 are employed. The nucleation of the particles begins with the addition of the reducer and the oxidizer, although it is also common to use seed particles. Homogeneous nucleation (also called primary nucleation in this work) dominates the beginning of the batch until the CMC is exceeded with the surfactant flow to the system and micellar nucleation (also called the secondary nucleation) becomes dominant around 15–20 min. The sharp peak present early in the batch resolves into a wider primary peak due to the size-dependent growth and the formation of a secondary peak. The PSD has two distinct modes at the end of the batch, a wide primary peak and a sharper secondary peak.

Simulation Case Studies

The proposed algorithm is tested on the PBE system described in the previous section. The system is run with the

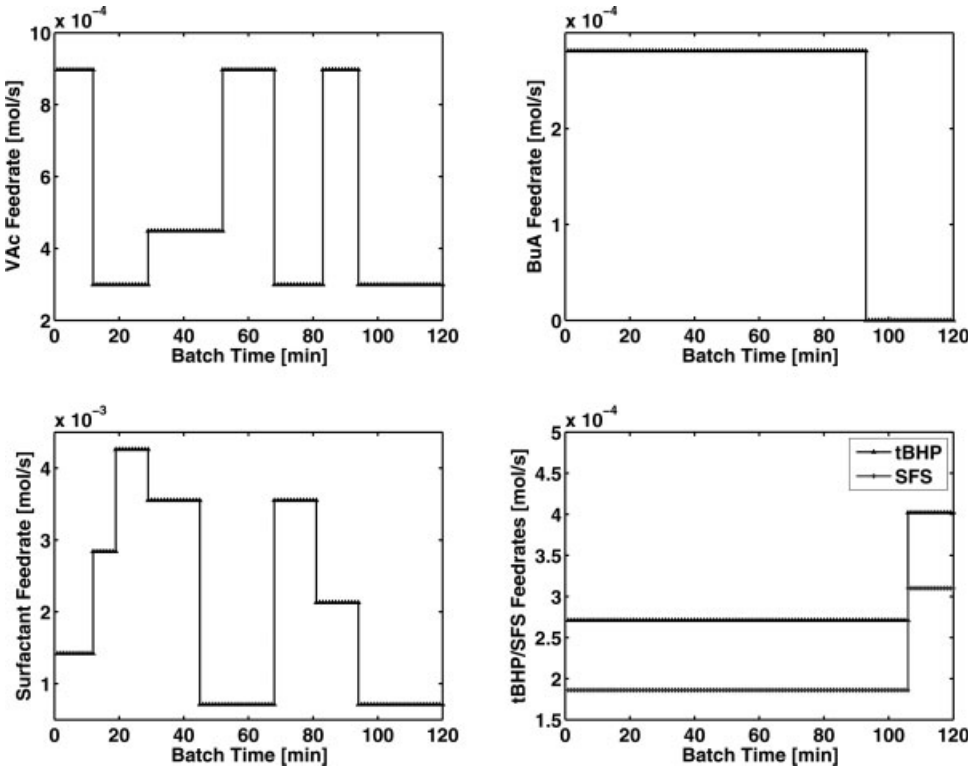

Figure 4. Nominal input profiles for the simulation studies.

same nominal input profiles, but the VAc kinetic parameters are altered to give a distinctly different endpoint distribution. The perturbations to the VAc kinetic parameters are a 25% increase to the propagation rate constants ($k_{p_{11}}$ and $k_{p_{12}}$). The effect of the perturbation on the endpoint w_{PSD} is illustrated in Figure 6. The increased VAc propagation rate causes the primary peak of the endpoint distribution to grow larger than the nominal and also affects the secondary peak height.

The manipulated variables that will be considered are the feed rates of the less active monomer VAc and the nonionic surfactant. These variables are selected due to their profound effect on the nucleation and growth regimes. The other feed

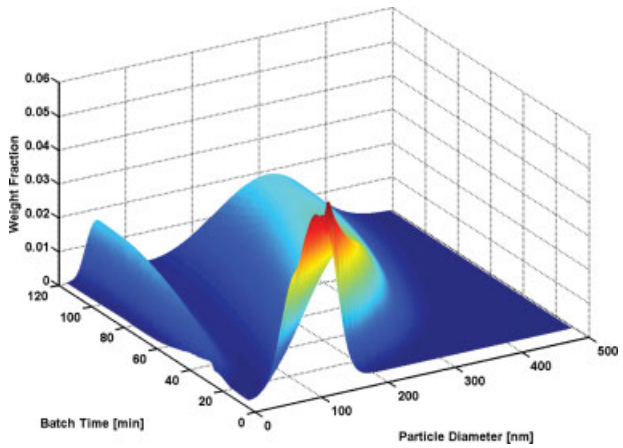

Figure 5. Evolution of the PSD with batch time during the nominal semibatch emulsion copolymerization of VAc/BuA, resulting with a bimodal PSD at the end of the batch.

[Color figure can be viewed in the online issue, which is available at www.interscience.wiley.com.]

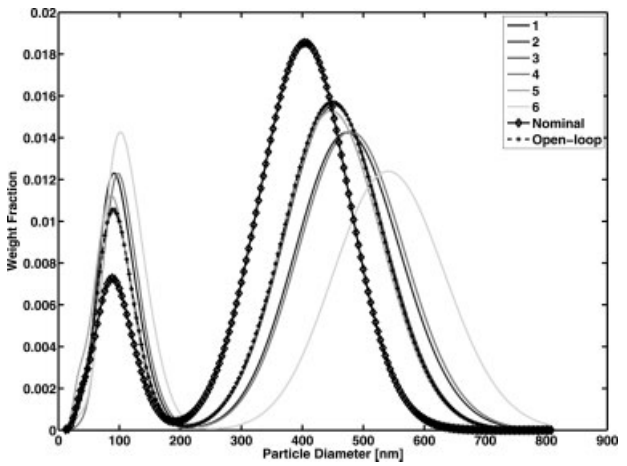

Figure 6. Endpoint w_{PSD}s of the open-loop training batches and the nominal (target) distribution for the first simulation case study.

The batch history consists of six batches for which the feed rate profiles are perturbed randomly.

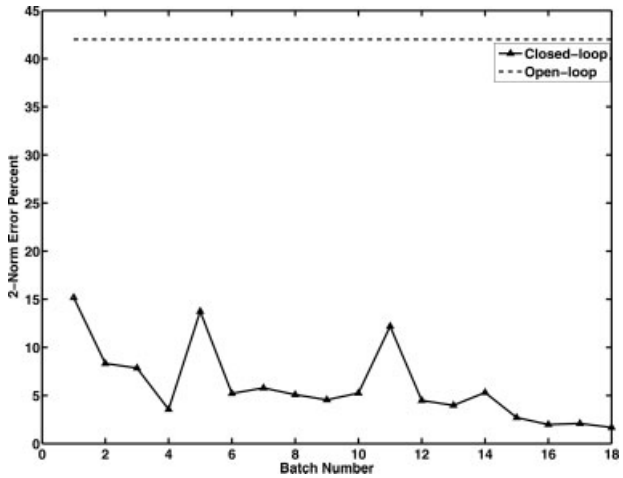

Figure 7. 2-norm error percentages of the controlled batches by the batch-to-batch controller in the first simulation case study.

The dashed line represents the error norm of the unregulated batches.

rate profiles are not considered to keep the number of decision variables as low as possible. A low number of optimized variables results with an effective solution of the optimization problem and manageable PLS models. A high number of decision variables may require more training experiments that cover a broader decision variable space, which may not be feasible due to the operational constraints. A critical parameter in the control methodology is the number of decision times. Three decision times are considered in this study, the first decision time is before the batch (0th min) and the other two decision times are during the batch at the 29th and 42nd minutes. At these two decision times during the batch, the measured outputs from the 2nd and 3rd w_{PSD} measurements are utilized together with the 29th- and 42nd-min solids content estimations. The decision times are selected to be relatively early during the batch in order for these input changes to have sufficient effect on the outcome. The PLS models for each decision time are selected to have a memory of the 12 most recent batches. To create an initial database of batches, only six training batches are simulated. In these training batches, VAc and surfactant feed rate profiles are perturbed randomly at the selected decision times. The effect of these random input changes are illustrated in Figure 6. An important point to note in this figure is the dissimilarity of the nominal distribution to the endpoint w_{PSD}s of the training batches. The target distribution is clearly out of the region that is covered by the endpoint distributions of the training batches.

In Figure 7, the 2-norm error percentages of the controlled batches are shown. The 2-norm error percentage is calculated as:

$$\text{2-norm error percent} = \frac{\left\| w_{\text{PSD target}} - w_{\text{PSD closed}} \right\|_2}{\left\| w_{\text{PSD target}} \right\|_2} \times 100$$

The controlled outputs of the system are the positions and heights of the tracer elements of the distribution for the size ranges 0–168 nm and 168–800 nm, creating a total number of 12

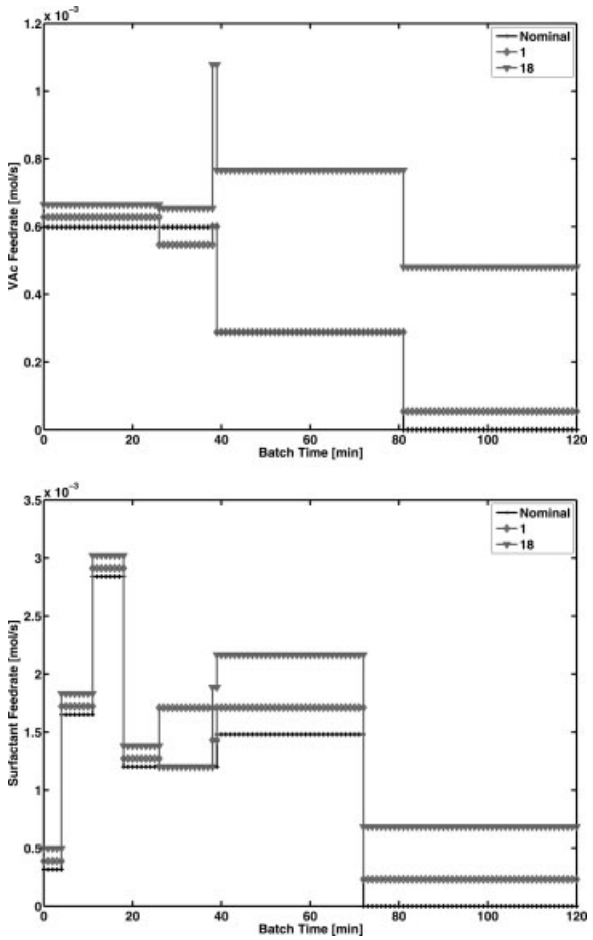

Figure 8. VAc and surfactant input profiles of the nominal, 1st and the 18th batches for the first simulation case study.

The controller is manipulating the input profiles to correct for the VAc kinetic parameter perturbations.

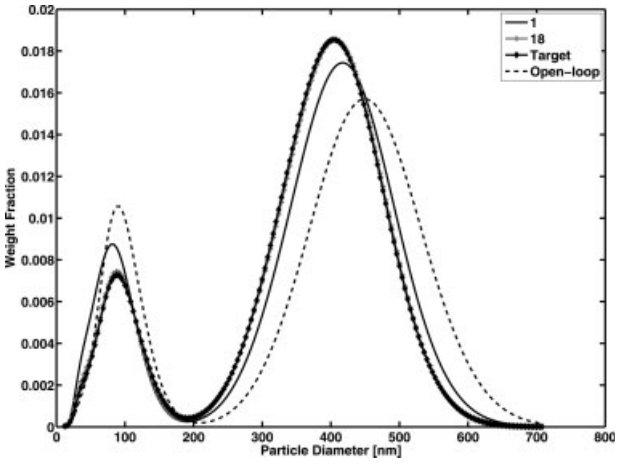

Figure 9. w_{PSD}s of the controlled batches in the first simulation case study.

The controller is able to approach the target w_{PSD} beginning with the first batch.

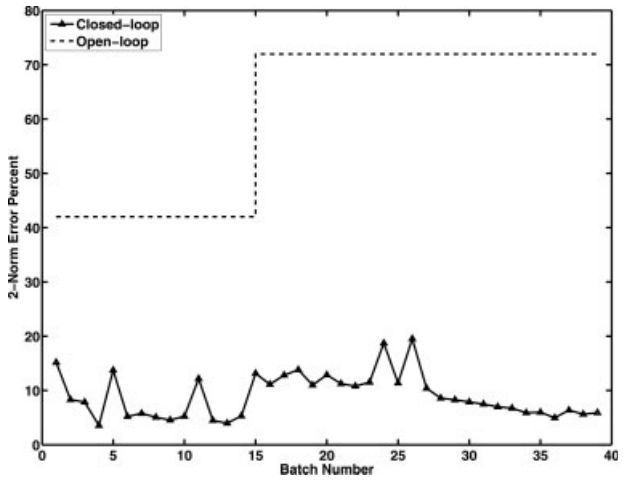

Figure 10. 2-norm error percentages of the controlled batches by the batch-to-batch controller in the second simulation case study.

The dashed line represents the error norm of the unregulated batches.

outputs. The controller weights are 90 for the six position outputs, 50 for the six height outputs, and one for the input changes:

$$\Gamma = \mathrm{diag}([90 \quad \cdots \quad 90 \quad 50 \quad \cdots \quad 50])$$
$$\Lambda_k = I_{2(3-k)}$$

where Λ_k is the weighting matrix for the kth decision time. The characterization of the tracer elements by the positions and the weight fractions (heights) enables separate weighing of these features in the controller objective function. This may be desirable in a process where the average sizes of each mode of the endpoint distribution are more important than the weight fraction of these modes or vice versa. After each batch, the number of latent variables for the new PLS models are determined by cross-validation to result with the best prediction performance. Once the batch history reaches 12 batches, the expansion of the predictor and the output

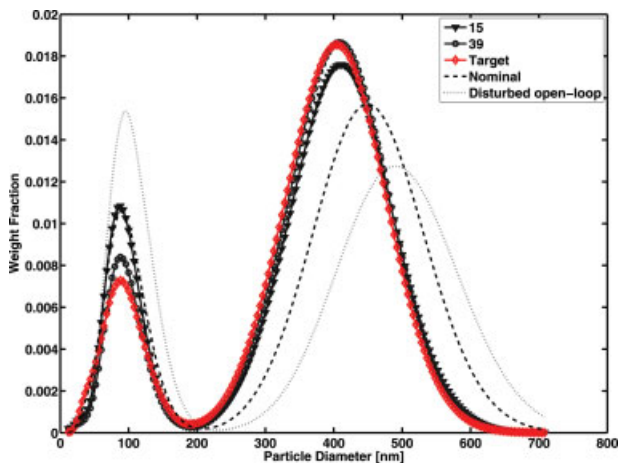

Figure 11. w_{PSD}s of the controlled batches in the second simulation case study.

The controller is still able to regulate the w_{PSD} to its target after a persistent operational disturbance introduced after the 15th batch. [Color figure can be viewed in the online issue, which is available at www.interscience. wiley.com.]

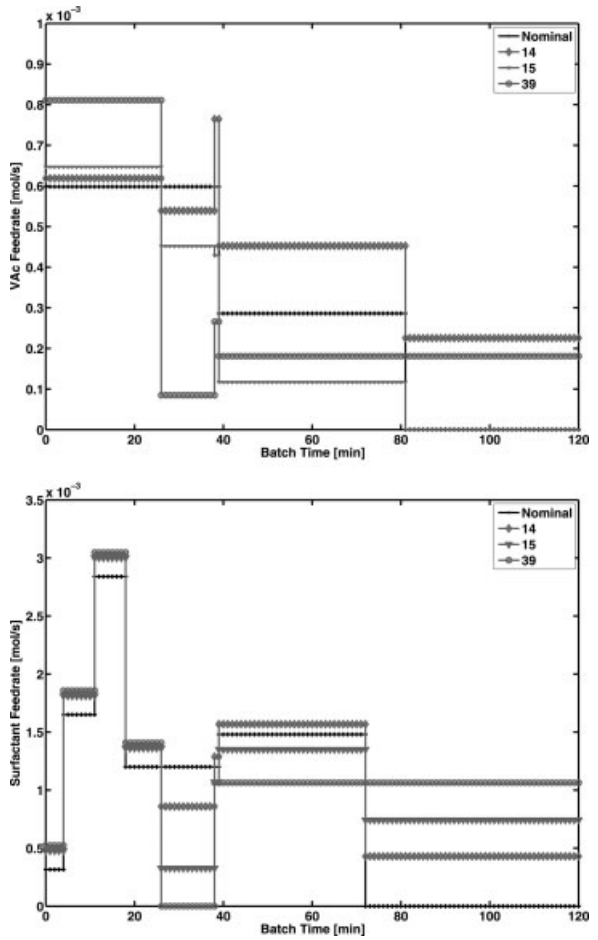

Figure 12. VAc and surfactant input profiles of the nominal, 14th, 15th, and 39th batches for the second simulated disturbance case.

The controller is manipulating more at the second decision time to reject the initial VAc disturbance introduced after the 15th batch.

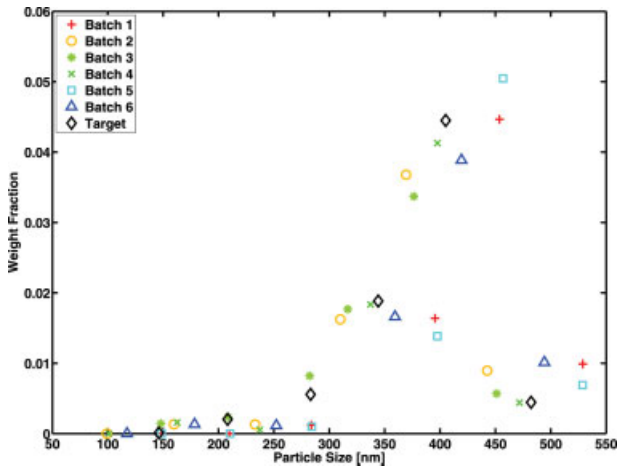

Figure 13. Tracer elements of the open-loop training batches and the target distribution in the first experimental case study.

[Color figure can be viewed in the online issue, which is available at www.interscience. wiley.com.]

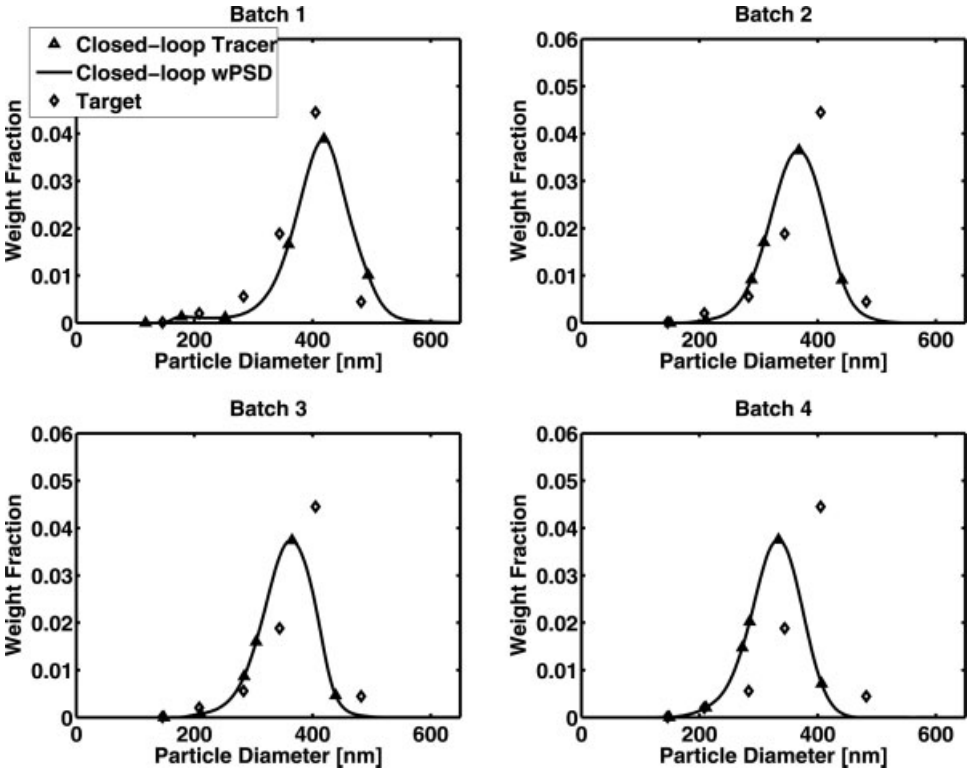

Figure 14. Endpoint PSDs and the tracer elements of the closed-loop batches 1–4 and the target tracer elements in the first experimental case study.

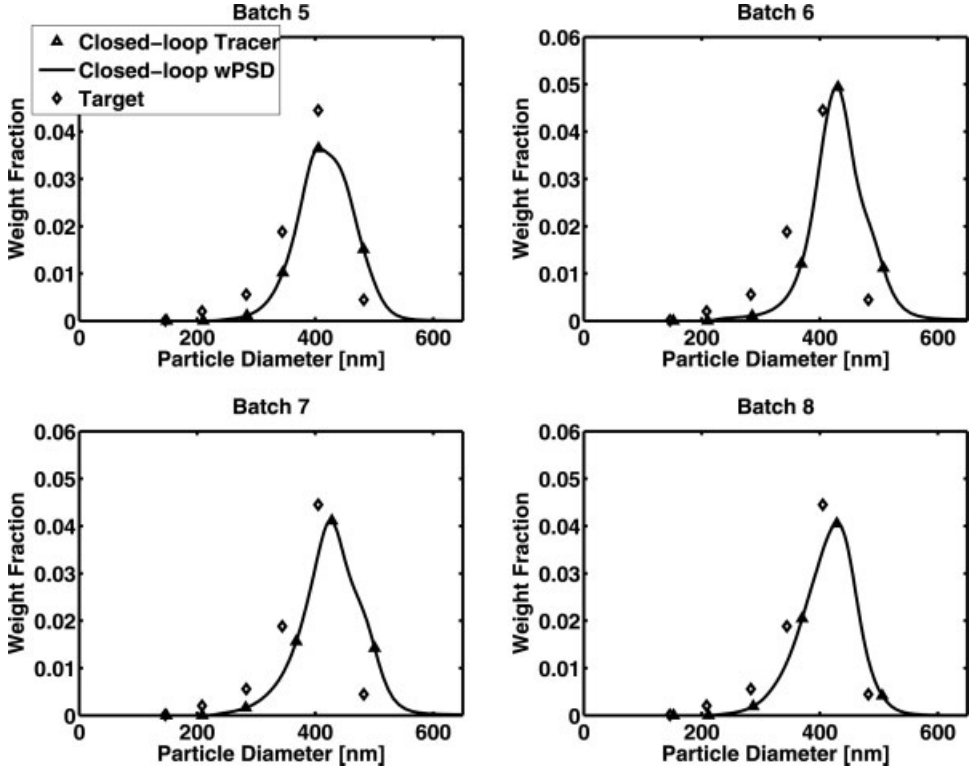

Figure 15. Endpoint PSDs and the tracer elements of the closed-loop batches 5–8 and the target tracer elements in the first experimental case study.

blocks are stopped and the models are constructed with only the most recent 12 batches. The input profiles for these simulations are presented in Figure 8. It can be inferred from the closed-loop profiles that the controller is able to determine the direction of change for each of the inputs properly beginning with the first batch. The VAc and the surfactant profiles are fine-tuned considerably by the controller until the 18th batch.

It can be seen in Figure 9 that the algorithm is successful in regulating the endpoint w_{PSD} to its target. The algorithm is able to get very close to the target w_{PSD} with the first batch, utilizing a PLS model of only six batches that have dissimilar w_{PSD}s to the target. The 2-norm error of the first batch is less than half of the open-loop error. At the fourth batch, the 2-norm error drops down to less than 5%. Normally a no-control zone of 5% would be selected for practical applications of the proposed algorithm. In such a case, the rest of the batches after the fourth batch would have had the same endpoint w_{PSD}, which is sufficiently close to the target as can be seen in Figure 9. The increase in the 2-norm error at the 5th and 11th batches is probably due to the aggressive tuning of the controller coupled with the low number of training batches. Ultimately, at the 18th batch, the 2-norm error drops down to less than 2%. In Figure 9, it is seen that the endpoint w_{PSD} of even the 1st batch is very close to the target and the final w_{PSD} of the 18th batch is almost exactly the same as the target distribution.

The second case study that is conducted on the simulated system aimed to test the adaptation of the algorithm to changing plant conditions or persistent operational disturbances. In the simulated disturbance scenario, the initial VAc charge to the reactor is decreased by 25% beginning with the 15th batch. The plant model and controller tunings are kept the same as the previous case study. The 2-norm error percentages of the closed-loop batches are presented in Figure 10. Even though the 2-norm error increases with the introduction of the disturbance at the 15th batch, the controller is able to keep the system under control and the error is less than 20%. The main reason behind the quick adaptation of the controller to the disturbance is the use of on-line measurements to take control actions during the batch.

The controller continues to move the endpoint distributions closer to the target from batch to batch. The oscillations in the 2-norm error around the 24th and 26th batches are due to the aggressive tuning of the controller. Also, a smaller window of history of batches can be used to improve the performance against unexpected persistent disturbances possibly at the expense of a lower model performance. Eventually, the algorithm is able to reduce the 2-norm error to 5%. The w_{PSD}s of the closed-loop batches are presented in Figure 11.

The extensive effect of the disturbance that hits the system at batch 15 can be seen in the disturbed w_{PSD} in Figure 11. Also, it is clear that the controller is able to keep the endpoint w_{PSD}s sufficiently near to the target distribution throughout the batches. The input profiles of the batches 14, 15, and 39 are presented in Figure 12. It can be seen that the controller is mainly changing the input profiles at the second decision time to reject the initial VAc disturbance showing the necessity of in-batch control.

Experimental Case Studies

The developed controller methodology is tested on the experimental system described in "Closed-loop experimental system" section. The main goal of the controller is to reach a target distribution characterized by tracer elements. The same controller structure from the simulation studies is utilized in this section. However, the on-line tracer element measurements during the batch use a single size range unlike the simulation study, where the collected measurements were characterized by tracer elements of two size ranges. The reason for this choice is that the evolution of the distribution in the experimental system exhibits unimodal characteristics during the second and third decision times. For the characterization of the endpoint distribution, two size ranges of 0–210 nm and 210–650 nm are utilized. The controller tuning is similar to the simulation study, where the position deviations have twice more penalty compared to the height deviations. The controller objective function weights are as follows:

$$\Gamma = \mathrm{diag}([20 \quad \cdots \quad 20 \quad 10 \quad \cdots \quad 10])$$
$$\Lambda_k = I_{2(3-k)}$$

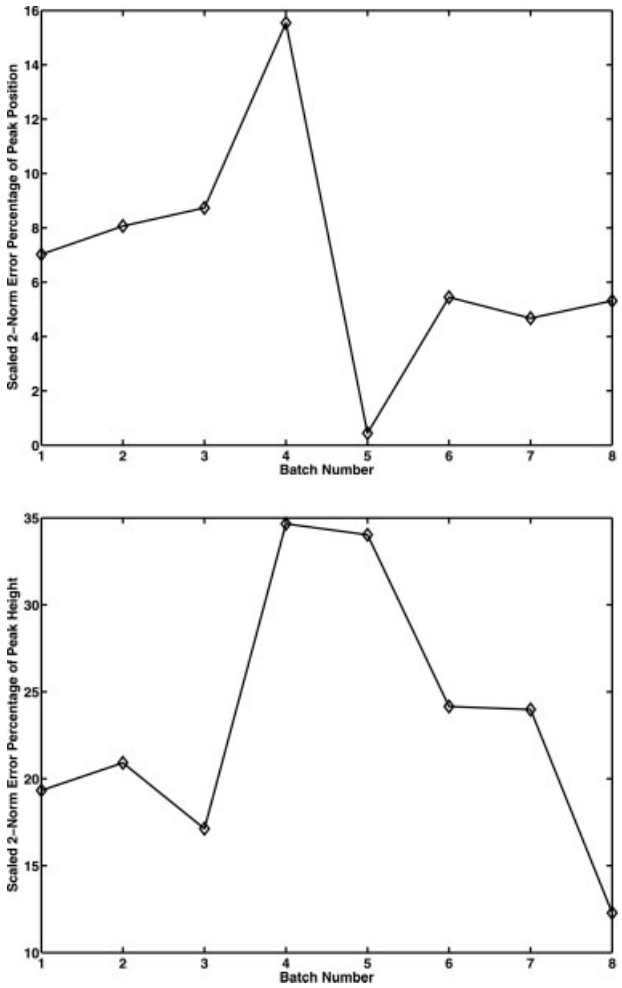

Figure 16. 2-norm error percentages of the tracer positions (top plot) and 2-norm error percentages of the tracer heights (bottom plot) in the first experimental case study.

The controller gathers enough information about the system after the first 4 batches and achieves control beginning with the 5th batch.

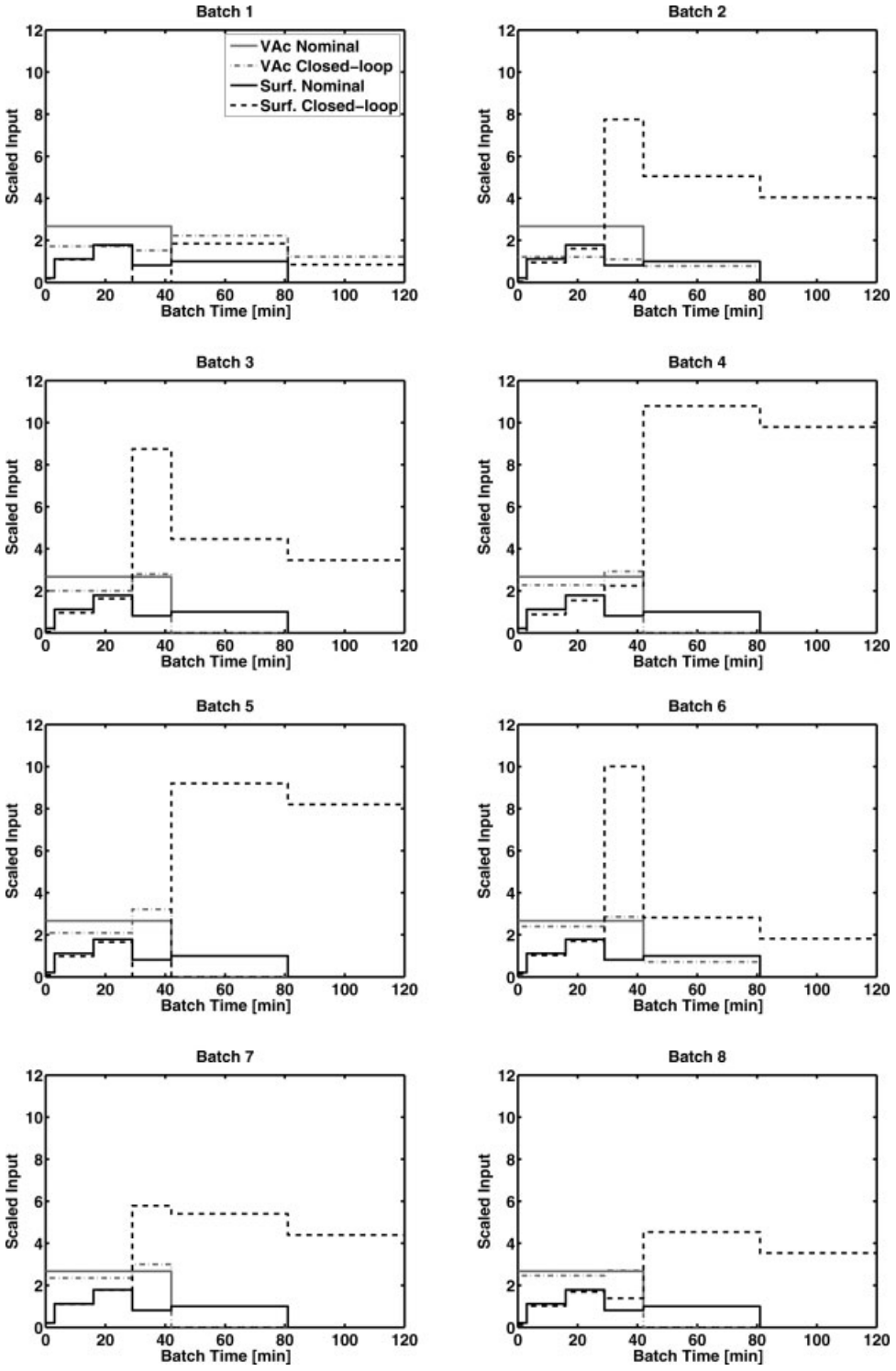

Figure 17. Closed-loop and nominal feed rate profiles of VAc and surfactant for batches 1–8 in the first experimental case study.

The feed rates are scaled by their base values presented in Table 1.

Six training batches are utilized in the first experimental case study. As was practiced in the simulation study, the nominal input profiles of VAc and surfactant were perturbed to obtain a batch history of the process. The tracer element locations of the endpoint distributions of these six training batches and the target tracer elements are presented in Figure 13. Although there are some distributions in the training database that have moderately close tracer elements to the target for each size range, the training database does not include any single distribution that has similar tracer

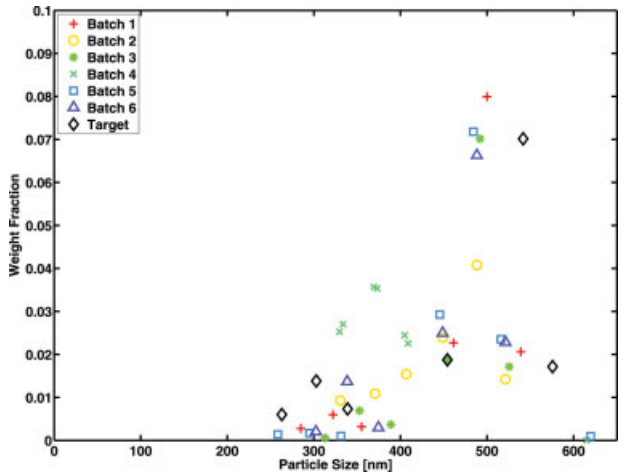

Figure 18. Tracer elements of the open-loop training batches and the target distribution in the second experimental case study.

[Color figure can be viewed in the online issue, which is available at www.interscience.wiley.com.]

elements to the target elements for both of the size ranges. The endpoint distributions of the first four batches and the target tracer elements are presented in Figure 14. Although batch 1 seems to exhibit a distribution with the tracer elements close to their target, the endpoint distributions of batches 2, 3, and 4 seem to move away from the target. This is most likely due to the insufficiency of the process knowledge obtained from the training batches.

However, once the controller has gathered enough knowledge of the system and is able to construct improved PLS models of the process, the performance of the controller improves significantly as presented in Figure 15. In batch 5, it is seen that the controller achieves almost perfect control of the tracer element positions ($y_{pos,1}$ through $y_{pos,6}$). This can also be seen in Figure 16, where the 2-norm error percentages of the tracer element positions are presented. Although perfect position control is achieved in batch 5, the control is less successful in terms of tracer element heights as presented in Figure 16. At this stage, it was decided that the controller tuning was too aggressive, causing the controller to focus solely on the tracer element positions. After detuning of the controller it can be seen that the distributions and their respective tracer elements move closer to their targets in Figure 15. In batch 8, both the positions and the heights of the tracer elements are regulated successfully.

The input profiles for all the closed-loop batches are presented in Figure 17. Beginning with batch 1, the surfactant feed rate profile is raised after the second decision time. In the final closed-loop batch, the surfactant feed rate is slightly increased at the second decision time and increased more at the third decision time. The correct direction of change for the VAc feed rate has been evaluated correctly by the controller beginning with batch 1. However, the system is very sensitive to VAc feed rate during the beginning of the batch. Therefore, for the rest of the closed-loop batches, the controller can be considered to be fine-tuning the VAc feed rate profile.

A second experimental case study is carried out to further identify the performance limits of the proposed control meth-

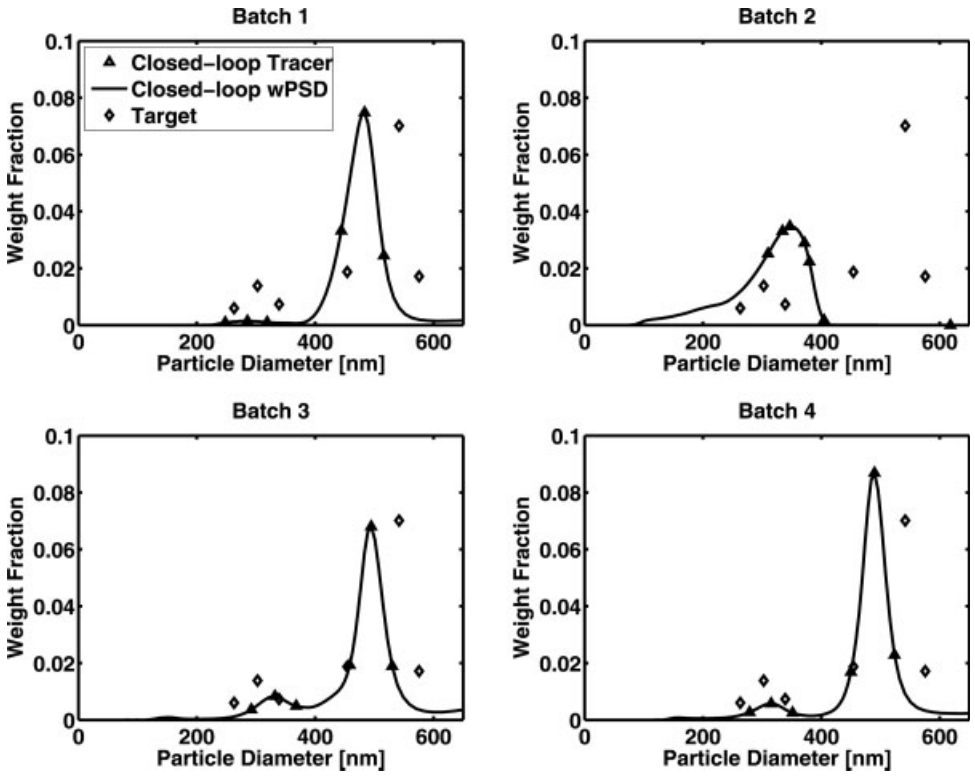

Figure 19. Endpoint PSDs and the tracer elements of the closed-loop batches 1–4 and the target tracer elements in the second experimental case study.

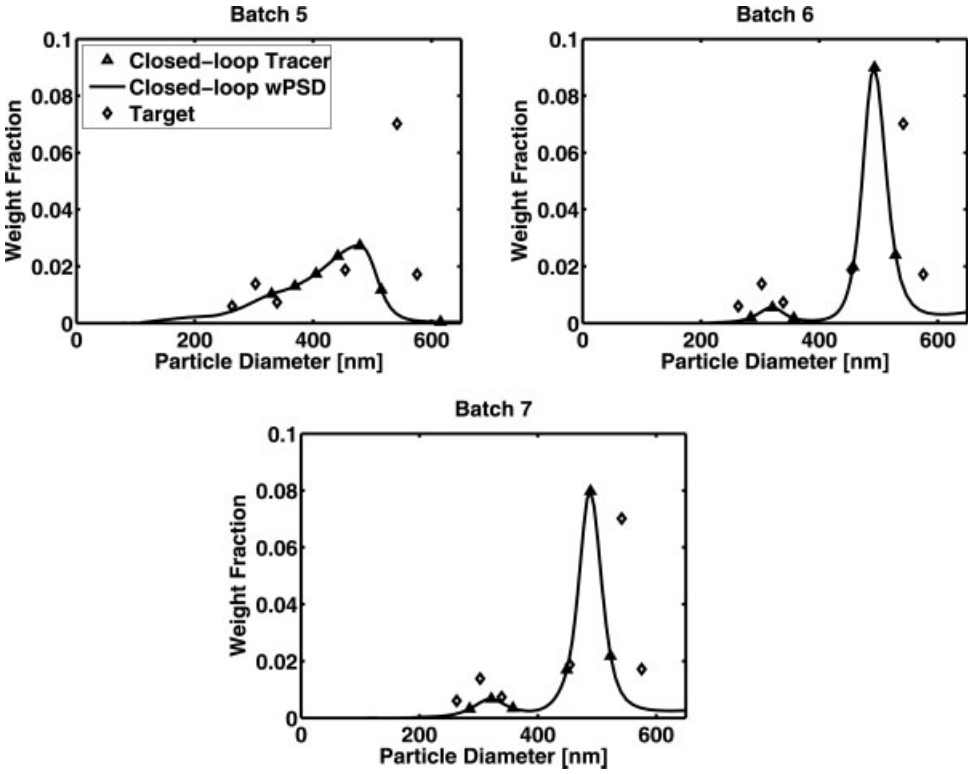

Figure 20. Endpoint PSDs and the tracer elements of the closed-loop batches 5–7 and the target tracer elements in the second experimental case study.

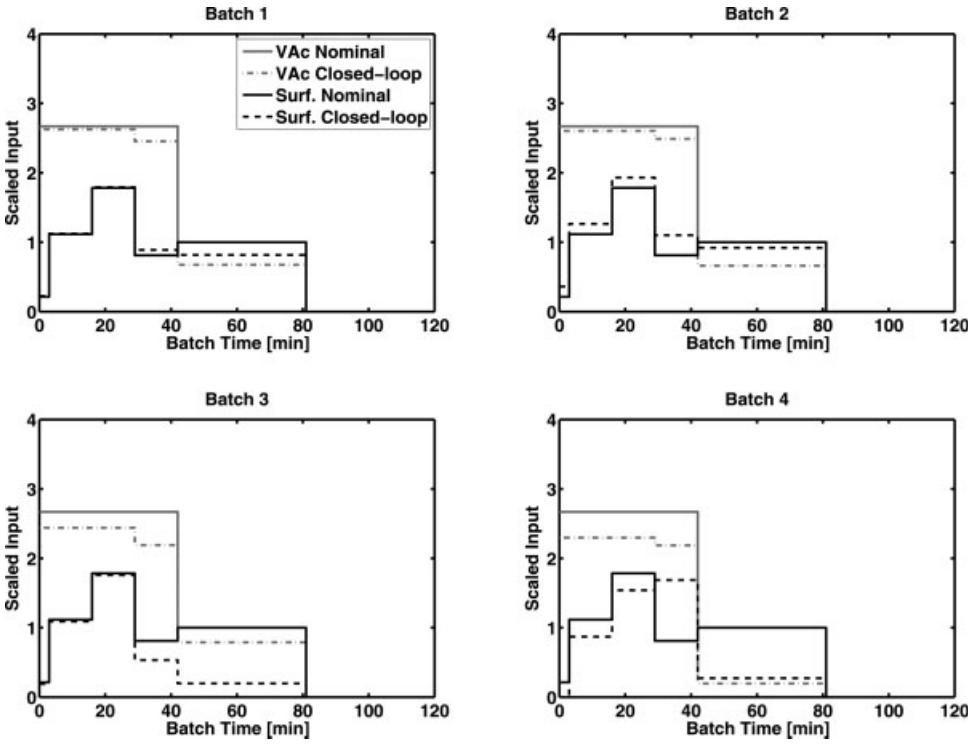

Figure 21. Closed-loop and nominal feed rate profiles of VAc and surfactant for batches 1–7 in the second experimental case study.

The feed rates are scaled by their base values presented in Table 1.

odology. The target bimodal PSD for this case study is selected to be away from the training database on both modes of the distribution to challenge the controller. In an industrial application, this might represent a novel product formulation. The tracer elements of the six training batches for the second case study are presented in Figure 18. It can be seen that the target tracer elements are away from the region covered by the elements of the training batches. The target elements trace a distribution that has a higher secondary peak and a wider primary peak than all the batches in the training dataset.

The endpoint size distributions of the first four closed-loop batches and the target elements are shown in Figure 19. In batch 1, the controller is able to match the positions of the tracer elements closely; also the heights of the tracer elements of the primary peak are controlled satisfactorily. However, the tracer element heights of the secondary peak and the tracer element positions of the primary peak are not controlled tightly. While trying to correct for these discrepancies, the controller overshoots and moves the distribution to very small size ranges. However, in batches 3 and 4, the controller is able regulate all tracer elements better than the first two batches although the primary peak is still not as wide and the secondary peak is not as high as the target tracer elements. The improvement observed in these batches is very likely the result of the improving quality of the PLS models, β_1, β_2, and β_3.

The controller algorithm overshoots again in batch 5 in an attempt to move the secondary peak closer to the target positions as shown in Figure 20. For the rest of the batches, the controller regulates the distributions to the best of its ability but cannot achieve the ultimate goals of widening the primary peak and increasing the maximum weight fraction of the secondary peak. A likely reason for this is the unreachability of the target tracer elements. The input profiles of all the batches for the second case study are presented in Figure 21. The 2-norm error percentages for the tracer element positions and heights are presented in Figure 22. There is a downward trend in both the height and the position error norms and the oscillatory behavior suggests that the controller is tuned aggressively.

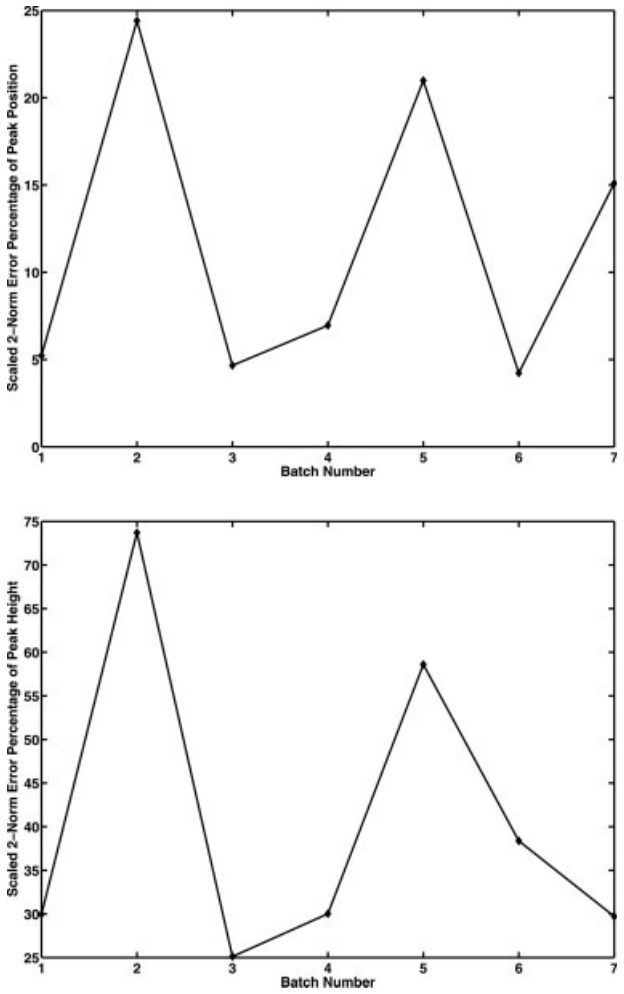

Figure 22. 2-norm error percentages of the tracer positions (top plot) and 2-norm error percentages of the tracer heights (bottom plot) in the second case study.

Conclusions

A batch-to-batch methodology incorporating in-batch on-line measurements to regulate the endpoint distribution in emulsion polymerization is presented in this work. In the proposed approach, the high dimensionality of the process is reduced by a novel method, where characteristic points on the distribution are tracked instead of the full-PSD. PLS models are utilized in an MPC framework to regulate the positions and heights of these characteristic points to their targets end of the batch. Three decision times are used to make changes to the profiles of VAc and surfactant feed rates. The first decision time constitutes the batch-to-batch component of the presented algorithm and the other two decision times have both batch-to-batch and in-batch components. The efficacy of the proposed algorithm is demonstrated by two simulation and two experimental case studies. In the simulation case studies, the algorithm proved to be a reliable method for regulating the endpoint distribution. The use of on-line measurements proved to be beneficial for rejecting a persistent disturbance that became active after certain number of batches was run. In the first experimental case study, the developed controller, utilizing the experimental training database of six batches, was able to attain the target tracer element positions and weight fractions very closely at the end of an eighth batch run. A second experimental case study was established in order to better determine the performance limits of the proposed algorithm. In this second case, the selected target was most likely unreachable and thus the aggressively tuned controller struggled to move the tracer elements to their targets. These results point to both the promise of the method and the practical limitations for implementation.

Notation

$k_{p_{ij}}$ = rate constant for propagation of polymer type i with monomer j
m_T = total mass of reactants in the reactor
M_i = moles of monomer i in the reactor

$[M_i]_p$ = concentration of monomer i in the particles
$[M_i]_w$ = concentration of monomer i in the aqueous phase
MW_i = molecular weight of monomer i
p_i = probability that a radical is of type i in the particles
r = particle radius
$V_{m_i}^T$ = total volume of monomer i fed to the reactor until current time

Greek letters

ρ_{latex} = density of the latex
ρ_{m_i} = density of monomer i
Γ = diagonal weighting matrix for the controller error
Λ_k = diagonal weighting matrix for the controller inputs at the kth decision time ($k = 0, 1, 2$)

Literature Cited

1. Shikata T, Niwa H, Morishima Y. Viscoelastic behavior of bimodal suspensions. *J Rheol*. 1998;42:765–780.
2. Tzitzinou A, Keddie JL, Geurts JM, Peters ACIA, Satguru R. Film formation of latex blends with bimodal particle size distributions: Consideration of particle deformability and continuity of the dispersed phase. *Macromolecules*. 2000;33:2695–2708.
3. Colombini D, Hassander H, Karlsson OJ, Maurer FHJ. Influence of the particle size and particle size ratio on the morphology and viscoelastic properties of bimodal hard/soft latex blends. *Macromolecules*. 2004;37:6865–6873.
4. Arevalillo A, do Amaral M, Asua J. M. Rheology of concentrated polymeric dispersions. *Ind Eng Chem Res*. 2006;45:3280–3286.
5. Kiparissides C. Challenges in particulate polymerization reactor modeling and optimization: A population balance perspective. *J Process Contr*. 2006;16:205–224.
6. Ramkrishna D. *Population Balances*. San Diego: Academic Press, 2000.
7. Dimitratos J, Elicabe G, Georgakis C. Control of emulsion polymerization reactors. *AIChE J*. 1994;40:1993–2021.
8. Richards JR, Congalidis JP. Measurement and control of polymerization reactors. *Comput Chem Eng*. 2006;30:1447–1463.
9. Semino D, Ray WH. Control of systems described by population balance equations. I. Controllabity analysis. *Chem Eng Sci*. 1995;50:1805–1824.
10. Semino D, Ray WH. Control of systems described by population balance equations. II. Emulsion polymerization with constrained control action. *Chem Eng Sci*. 1995;50:1825–1839.
11. Wang Y, Doyle FJ III. Reachability of particle size distribution in semibatch emulsion polymerization. *AIChE J*. 2004;50:3049–3059.
12. Chiu T, Christofides PD. Nonlinear control of particulate processes. *AIChE J*. 1999;45:1279–1297.
13. Kalani A, Christofides PD. Simulation, estimation and control of size distribution in aerosol processes with simultaneous reaction, nucleation, condensation and coagulation. *Chem Eng Sci*. 2002;26:1153–1169.
14. Shi D, El-Farra NH, Li M, Mhaskar P, Christofides PD. Predictive control of particle size distribution in particulate processes. *Chem Eng Sci*. 2006;61:268–281.
15. Crowley TJ, Meadows ES, Kostoulas E, Doyle FJ III. Control of particle size distribution described by a population balance model of semibatch emulsion polymerization. *J Process Cont*. 2000;10:419–432.
16. Lee K, Lee JH, Yang DR, Mahoney AW. Integrated run-to-run and on-line model-based control of particle size distribution in semibatch precipitation reactor. *Comput Chem Eng*. 2002;26:1117–1131.
17. Doyle FJ III, Harrison CA, Crowley TJ. Hybrid model-based approach to batch-to-batch control of particle size distribution in emulsion polymerization. *Comput Chem Eng*. 2003;27:1153–1163.
18. Flores-Cerrillo J, MacGregor JF. Within-batch and batch-to-batch inferential-adaptive control of semibatch reactors: a partial least squares approach. *Ind Eng Chem Res*. 2003;42:3334–3345.
19. Park MJ, Dokucu MT, Doyle FJ III. Regulation of the emulsion particle size distribution to an optimal trajectory using partial least squares model-based predictive control. *Ind Eng Chem Res*. 2004;43:7227–7237.
20. Alhamad B, Romagnoli JA, Gomes VG. On-line multi-variable predictive control of molar mass and particle size distributions in free radical emulsion polymerization. *Chem Eng Sci*. 2005;60:6596–6606.
21. Rajabi-Hamane M, Engell S. Time optimal production of a specified particle size distribution in emulsion polymerization. *Chem Eng Sci*. 2007;62:5282–5289.
22. Geladi P, Kowalski BR. Partial least-squares regression: a tutorial. *Anal Chim Acta*. 1986;185:1–17.
23. de Jong S. SIMPLS: an alternative approach to partial least squares regression. *Chemometr Intell Lab*. 1993;18:251–263.
24. Wise BM, Gallagher NB, Bro R, Shaver JM. *PLS Toolbox 3.5 for Use with MATLAB*. Manson, WA: Eigenvector Research Technologies, 2005.
25. Kourti T. Multivariate dynamic data modeling for analysis and statistical process control of batch processes, start-ups and grade transitions. *J Chemometr*. 1993;17:93–109.
26. Elizalde O, Leal GP, Leiza JR. Particle size distribution measurements of polymeric dispersions: a comparative study. *Part Part Syst Char*. 2000;17:236–243.
27. Schneider M, McKenna TF. Comparative study of methods for the measurement of particle size and particle size distribution of polymeric emulsions. *Part Part Syst Char*. 2002;19:28–37.
28. Vicente M, Leiza JR, Asua JM. Simultaneous control of copolymer composition and MWD in emulsion copoymerization. *AIChE J*. 2001;47:1594–1606.
29. Saenz DeBuruaga I, Arotcarena M, Armitagea PD, Gugliotta LM, Leiza JR, Asua JM. On-line calorimetric control of emulsion polymerization reactors. *Chem Eng Sci*. 1996;51:2781–2786.
30. Immanuel CD, Cordeiro CF, Sundaram SS, Meadows ES, Crowley TJ, Doyle FJ III. Modeling of particle size distribution in emulsion co-polymerization: Comparison with experimental data and parametric sensitivity studies. *Comput Chem Eng*. 2002;26:1133–1152.
31. Immanuel CD, Doyle FJ III. Computationally efficient solution of population balance models incorporating nucleation, growth and coagulation: Application to emulsion polymerization. *Chem Eng Sci*. 2003;58:3681–3698.

Manuscript received Jan. 30, 2008, revision received May 27, 2008, and final revision received July 17, 2008.